Chapter 3

Room Temperature Crystal Structure and High Temperature Structural and Magnetic Phase Transitions in $Sr(Fe_{0.5}Nb_{0.5})O_3$ Ceramic

3.1 Introduction:

As discussed in Chapter 1, the $BiFeO_3$ ceramic is the most widely investigated multiferroic compound. The crystal structure, dielectric, ferroelectric and magnetic properties of $BiFeO_3$ are well investigated by earlier researchers and lots of literature is available for this compound. However, the $Sr(Fe_{0.5}Nb_{0.5})O_3$ ceramic is relatively less explored for the structure, phase transition, dielectric and magnetic properties. In view of this, we decided to investigate first the $Sr(Fe_{0.5}Nb_{0.5})O_3$ ceramic before characterizing the structure and properties of various compositions of the $(1-x)BiFeO_3$-$xSr(Fe_{0.5}Nb_{0.5})O_3$ solid solution. Further, the structure of SFN ceramic at room temperature is controversial. Different authors have reported different crystal structure at room temperature for SFN [Liu et al. (2007), Tezuka et al. (2000), Saha and Sinha (2006), Akhtar and Khan (2011), Rodriguez et al. (1985), Lufaso et al. (2006), Kruea-In et al. (2013)]. Rodriguez et al. (1985) have reported cubic structure for SFN at room temperature while Tezuka et al. (2000) reported orthorhombic (*Pnma*) structure. Saha and Sinha (2006) have reported monoclinic structure for SFN ceramic. Lufaso et al. (2006) reported tetragonal structure with *I*4/*mcm* space group for SFN samples with small amount of $Sr_{3.72}(Nb_{17}O_{26})$ impurity (JCPDS No. 87-2218). Akhtar and Khan (2011) have reported tetragonal structure in the *P*4*mm* space group. Thus, there is a need to resolve the controversial reports on the room temperature structure of SFN and determine the correct crystal structure. Further, several authors have studied the dielectric behaviour of SFN [Raevski et al. (2003), Liu et al. (2007), Saha and Sinha (2006)], but nothing has been reported about the high temperature magnetic phase transitions and magnetic properties. The high temperature structure and structural phase transition is also not well investigated for SFN.

This chapter present the results of our investigation on the crystal structure, dielectric, ferroelectric and magnetic behaviour of $Sr(Fe_{0.5}Nb_{0.5})O_3$ ceramic. We have resolved the controversial reports for the room temperature structure of $Sr(Fe_{0.5}Nb_{0.5})O_3$ ceramic using high quality phase pure samples. Rietveld structure refinement has been done to determine precisely the structural parameters and structural phase transition above room temperature in SFN. The structural and magnetic phase transitions investigated above room temperature reveals a structural phase transition around ~ 630K and a new magnetic phase transitions around ~708K, in this system. The high temperature structural phase transition was also confirmed by temperature dependence of Fe/NbO_6 octahedra tilt angle, integrated intensity of strongest superlattice reflection and differential scanning calorimetric (DSC) measurements.

3.2 Experimental

Pure perovskite phase $Sr(Fe_{0.5}Nb_{0.5})O_3$ (SFN) powder has been synthesized by solid state reaction method as discussed in Chapter 2. This fine powder was annealed at 873 K for 10 h to get rid of strains introducing during crushing. The XRD data in the temperature range 300K-850K was collected in the 2θ range 10^o-122^o at a step of 0.02^o using a high temperature attachment on Rigaku SmartLab high resolution X-ray diffractometer having Johansson $CuK\alpha_1$ optics. Absence of $CuK\alpha_2$ component in the diffraction patterns helps in unambiguous structure determination. For dielectric measurement, both sides of sintered pellets were cleaned carefully then silver paste were applied on flat surfaces and fired on at temperature 773K for 5 minutes. The dielectric permittivity (ε_r) and loss tangent ($\tan\delta$) of electroded pellets were measured in the temperature range 300K-850K using Nova Control (alpha-A) high performance impedance analyser. The magnetic field dependent magnetization (M-H loop) at room temperature and temperature dependent magnetization measurements (ZFC, FCC and

FCW) in the temperature range 300 K to 900 K at a low magnetic field of 500 Oe were carried out using a Quantum Design MPMS-3 system based on SQUID. Differential scanning calorimetry at a heating rate of 5 K/min was done by using Metller-Toledo DSC. FullProf Suite [Carvajal (2008)] was used for the Rietveld structure refinement of $Sr(Fe_{0.5}Nb_{0.5})O_3$ (SFN). Linear interpolation method was used to model the background for Rietveld refinements. Pseudo-Voigt peak shape function including anisotropic strain parameters was chosen to generate profile shape for the XRD peaks.

3.3 Results and Discussion

3.3.1 Room Temperature Crystal Structure of $Sr(Fe_{0.5}Nb_{0.5})O_3$ Ceramic

At room temperature, five different crystal structures for $Sr(Fe_{0.5}Nb_{0.5})O_3$ ceramic have been reported in the literature as discussed in Chapter 1. Rodriguez et al. (1985) have reported cubic structure for SFN at room temperature while many authors reported orthorhombic structure in the *Pnma* (*Pbnm*) space group [Liu et al. (2007), Tezuka et al. (2000), Kruea-In et al. (2013)]. Saha and Sinha (2006) reported monoclinic structure, however; the lattice parameter given by these authors is not consistent with the perovskite lattice parameters which clearly suggest that the structure reported by Saha and Sinha (2006) is incorrect. They reported the monoclinic lattice parameter as, a = 2.836 Å, b = 2.882 Å, c = 2.804 Å and the monoclinic angle $\beta = 92.83^0$. However, the lattice parameters for primitive perovskite structure are around ~ 4 Å or a multiple of it for bigger unit cells. Lufaso et al. (2006) performed Rietveld structure refinement for SFN using *I*4*/m* and *I*4*/mcm* space groups and concluded that SFN has tetragonal structure in *I*4*/mcm* space group. Later on, using Rietveld structure refinement, Akhtar and Khan (2011) reported tetragonal structure in the *P*4*mm* space group whereas many authors [Liu et al. (2007), Kruea-In et al. (2013)] reported that SFN has orthorhombic structure in *Pbnm* space group. Fig. 3.1 shows the room

temperature, high resolution powder X-ray diffraction pattern of $Sr(Fe_{0.5}Nb_{0.5})O_3$ ceramic in 2θ range 20^0 to 70^0. A clear superlattice reflection is seen in this figure around two theta value of 37.5 degree in addition to the peaks corresponding to the primitive perovskite cell. Presence of a superlattice reflection in the diffraction profile of SFN ceramic rejects the tetragonal *P*4*mm* space group reported by Akhtar and Khan (2011) as it corresponds to the primitive perovskite cell. Observation of clear splitting in the (200) pseudocubic reflection, rules out the cubic structure reported by Rodriguez et al. (1985). The other option from the reports of earlier authors is the orthorhombic structure in (*Pbnm*) space group [Liu et al. (2007), Tezuka et al. (2000), Kruea-In et al. (2013)]. However, a careful examination of the (111) pseudocubic XRD profile shown in the inset to the Fig. 3.1 suggests that there is no splitting and it appears as a singlet. This rule out the orthorhombic structure since (111) pseudocubic XRD profile show splitting as (202) and (022) doublet for the *Pbnm* (or *Pnma*) space group. Appearance of (111) pseudocubic XRD profile as singlet and the (200) XRD profile as doublet suggests a tetragonal structure for $Sr(Fe_{0.5}Nb_{0.5})O_3$. In view of this we refined the structure of SFN considering different plausible tetragonal space groups.

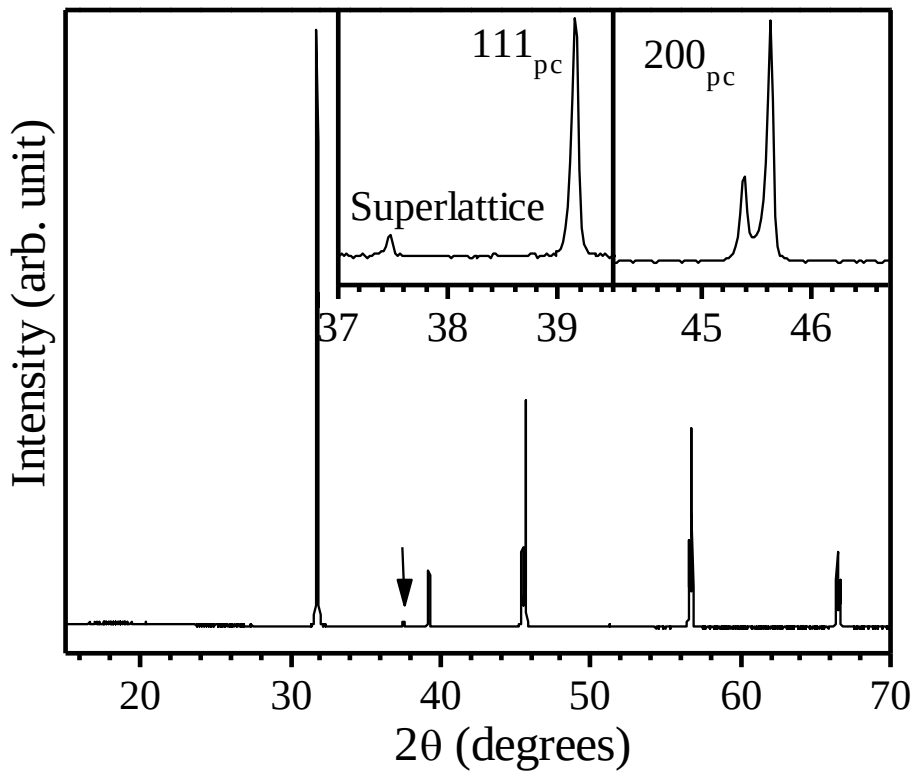

Figure 3.1 Powder XRD pattern of $Sr(Fe_{0.5}Nb_{0.5})O_3$ ceramic. A superlattice reflection at 37.5^o is marked with arrow. Insets show the zoomed portion of the XRD pattern.

The experimental XRD pattern was found to be accounted very well by the tetragonal *I4/mcm* space group. This confirms that the *I4/mcm* structure reported by Lufaso et al., (2006) in samples with small amount of impurity is also present for the single phase stoichiometric sample of SFN. For Rietveld structure refinement with tetragonal *I4/mcm* space group, the asymmetric unit of structure consists of four atoms in which, Sr occupies the 4b sites at (0.00, 0.50, 0.25) and the Fe/Nb on 4c sites at (0.0, 0.0, 0.0), while the remaining two type of oxygen ions are O(1) on 4a sites at (0.00, 0.0, 0.25) and O(2) on 8h sites at (0.25+ δ, 0.75+ δ, 0.00). Here the symbol 'δ' represents the refinable shift.

In Fig. 3.2, we present the Rietveld fits for some selected part of the XRD pattern of SFN by considering *I4/mcm* space group (upper panel). For the sake of

comparison we have also shown the Rietveld fit corresponding to the orthorhombic *Pbnm* space group (lower panel). As can be seen from this figure, for the *Pbnm* space group many superlattice reflections are expected (marked by arrows) which are absent in the experimental XRD pattern. In case of *I4/mcm* space group there is only one superlattice reflection around 37.5^{o} which is seen in both the experimental and Rietveld calculated patterns.

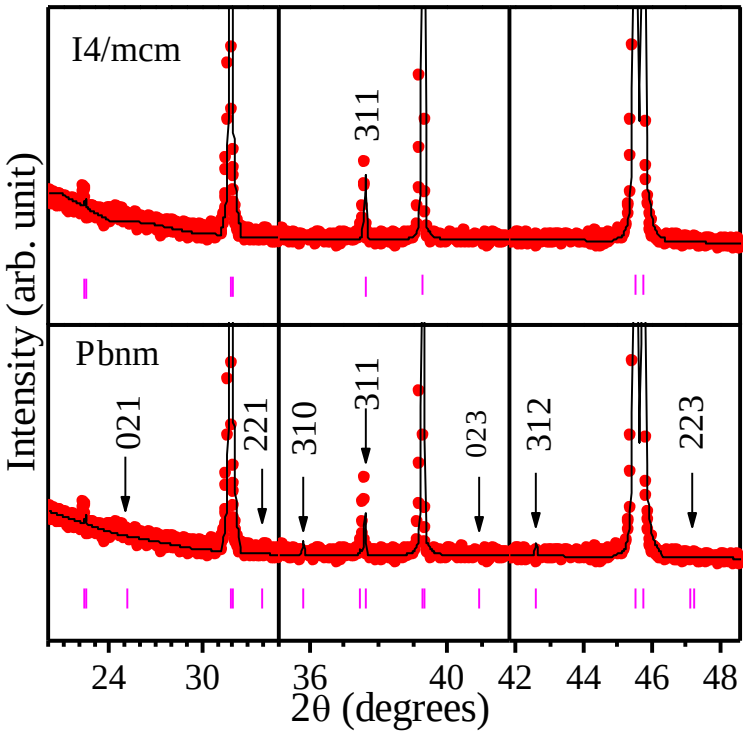

Figure 3.2 Rietveld fits for the selected XRD profiles of $Sr(Fe_{0.5}Nb_{0.5})O_3$ using tetragonal (*I4/mcm* space group, upper panel) and orthorhombic (*Pbnm* space group, lower panel) structures. The positions of superlattice reflections along with the indices, expected for orthorhombic structure with *Pbnm* space group, are marked by arrows. All the indices are written with respect to double cubic perovskite cell.

The superlattice reflection present in the diffraction profile of SFN is well fitted by *I4/mcm* space group. The absence of superlattice reflections corresponding to *Pbnm* space group and no splitting in (111) pseudocubic XRD profile in the XRD pattern of SFN, clearly rules out the possibility of *Pbnm* space group reported by earlier authors

[Liu et al. (2007)]. The tetragonal structure with *I4/mcm* space group has been reported for other similar double perovskite also like $Pr_{0.5}Sr_{0.5}MnO_3$, $SrFe_{0.75}Mo_{0.25}O_{3-\delta}$ and $Sr(Mn_{0.5}Ru_{0.5})O_3$ [Damay et al. (1998), Retuerto et al. (2012), Lufaso et al. (2004)]. The *Pbnm* space group belongs to $a^-a^-c^+$ tilt system. In this tilt system, neighbouring oxygen octahedra are rotated in anti-phase manner along [100], [010], whereas in-phase rotation about the [001] direction is followed by the octahedra. Due to out-of-phase tilts all the three pseudocubic cell parameters become double that causes the appearance of superlattice reflections whose Miller indices corresponding to the doubled cubic cell are designated by the three odd integers as 'ooo' [Glazer (1972) and (1975)]. On the other hand, in-phase tilts lead to the doubling of two cell parameters in the directions perpendicular to the tilt axis i.e. along two of the ⟨100⟩ directions. In this case, superlattice reflections have Miller indices designated by two odd (oo) and one even (e) integer (i.e. Miller indices are of 'ooe' type) [Glazer (1972) and (1975)]. In the $a^-a^-c^+$ tilt system, the antiparallel shift of 'A' cation in the neighbouring ABO_3 unit cells also causes the appearance of the superlattice reflections. The Miller indices for such superlattice reflections are designated by two even (ee) and one odd (o) integers, i.e., they have Miller indices of 'eeo' type [Glazer (1972) and (1975)]. If powder diffraction pattern of $Sr(Fe_{0.5}Nb_{0.5})O_3$ ceramic belong to the *Pbnm* space group with $a^-a^-c^+$ tilt system, one expects the appearance of superlattice reflections with 'ooo', 'ooe' and 'oee' indices due to the out-of-phase (a^-a^-) tilting of oxygen octahedra about [010] and [100] pseudocubic directions and in-phase (c^+) tilting of the octahedra about [001] direction and antiparallel cationic displacements, respectively. However, such superlattice reflections are not present in the experimental XRD pattern of SFN. For the tetragonal *I4/mcm* space group, which belongs to $a^oa^oc^-$ tilt system, the neighbouring oxygen octahedra rotate in antiphase manner about [001] direction. This kind of

rotation causes the doubling of elementary perovskite cell with the appearance of superlattice reflection along with characteristic splitting of main perovskite reflections. In case of $a^oa^oc^-$ tilt system, the Miller indices of the superlattice reflections with respect to the doubled cubic cell are designated by three odd integers as 'ooo' [Glazer (1972) and (1975)]. As shown in Fig. 3.2, the lone superlattice peak at $2\theta \approx 37.5^0$ bears (311) Miller indices with respect to the doubled cubic cell resulting from the antiphase tilting of the oxygen octahedra corresponding to $a^oa^oc^-$ tilt system in the tetragonal *I4/mcm* space group. At the positions of arrows in lower panel of Fig. 3.2, no superlattice peaks are seen having Miller indices, like (310) at $2\theta \approx 35.7^0$, (312) at $2\theta \approx 42.5^0$ characteristic of in-phase tilting of the oxygen octahedra in *Pbnm* space group. Further, prominent peaks like (021) at $2\theta \approx 25^0$, (221) at $2\theta \approx 33.7^0$, (023) at $2\theta \approx 40.75^0$, or (223) at $2\theta \approx 47.07^0$, expected for a characteristic of antiparallel cationic shift in pseudocubic directions, are also absent in the experimental XRD pattern. Hence on the basis of above discussions and the absence of several characteristic superlattice reflections corresponding to *Pbnm* space group in the diffraction pattern, we reject the reported orthorhombic structure for SFN ceramic in *Pbnm* space group. The correct crystal structure of SFN is confirmed to be tetragonal in the *I4/mcm* space group. Fig. 3.3 shows the Rietveld fit for the XRD pattern of SFN in the 2θ range 20^0 to 120^0 using tetragonal *I4/mcm* space group. It is evident from Fig. 3.3 that the overall fit for complete XRD pattern is also very good. The structural parameters obtained from the Rietveld structure refinement of SFN for *I4/mcm* space group are listed in Table 3.1.

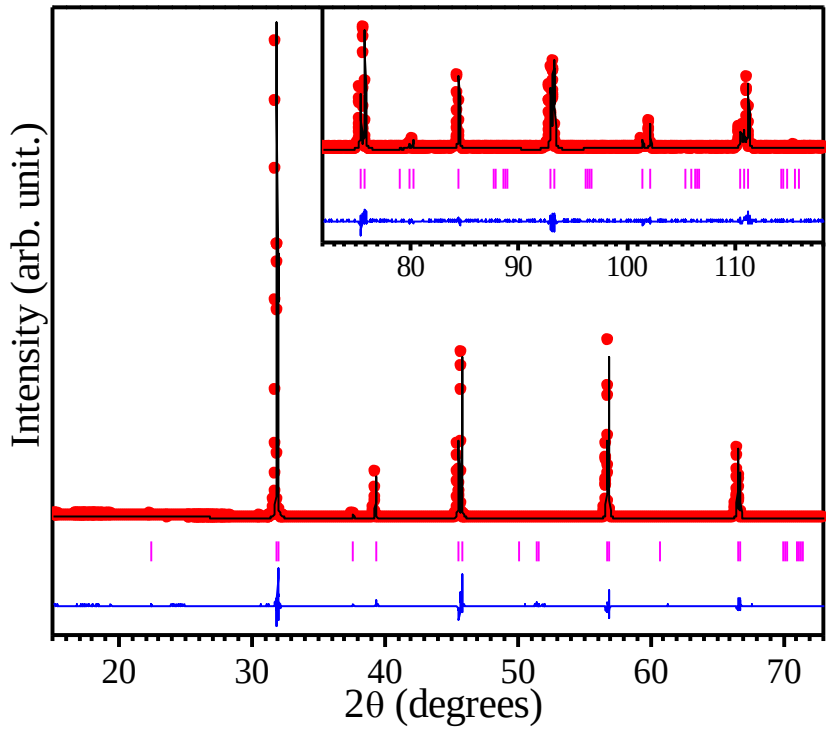

Figure 3.3 Observed (dots), Rietveld calculated (overlapping continuous plot) and difference (bottom curve) XRD profiles for $Sr(Fe_{0.5}Nb_{0.5})O_3$ ceramic at RT using tetragonal *I*4/*mcm* space group.

Table 3.1 Refined structural parameters of $Sr(Fe_{0.5}Nb_{0.5})O_3$ at room temperature, using tetragonal structure with *I*4/*mcm* space group.

Space group: *I*4/*mcm*				
Atoms	*x*	*y*	*z*	*B*(Å^2)
Sr	0.00	0.50	0.25	0.67(3)
Fe/Nb	0.00	0.00	0.00	0.25(3)
O1	0.00	0.00	0.25	0.01(5)
O2	0.223(6)	0.723(6)	0.0	0.9(1)
$a = b$ = 5.6086(8) (Å), c = 7.9713(3) (Å) R_p = 9.34, R_{wp} = 12, R_{exp} = 8.28				

3.3.2 Dielectric Studies on $Sr(Fe_{0.5}Nb_{0.5})O_3$ Ceramic

Fig. 3.4 (a) and (b) shows the temperature dependence of real part ε′(T) of the dielectric permittivity and loss tangent (tan δ) for SFN in the temperature range 300-800K at various frequencies from 1kHz to 9MHz. Two dielectric anomalies are seen at lower frequencies in the temperature dependence of the permittivity of SFN above room temperature. A zoomed portion of the real part of permittivity is shown in the inset of Fig. 3.4(a), from which, we can see that dielectric peaks flatten out as we go in the higher frequency region and finally disappear at 9MHz. This confirms that these anomalies appear due to extrinsic factors and are not related to any phase transition. However, a clear peak is seen even at higher frequencies, in temperature dependence of dielectric loss. Fig. 3.4 (c) shows the temperature dependence of imaginary part of modulus (M″) in the same frequency range. From the modulus (M″) formalism of dielectric relaxation of $Sr(Fe_{0.5}Nb_{0.5})O_3$, we have investigated the variation of relaxation time with temperature. As shown in Fig. 3.4 (d), the variation of relaxation time obeys the Arrhenius law, $\tau = \tau_0 \exp(E_a/kT)$, where, τ_0 is the pre-exponential factor, E_a is the activation energy and k is the Boltzmann's constant. The value of activation energy (E_a) and the pre-exponential factor (τ_0) thus calculated from the fitting are 0.776 eV and 4.4×10^{-15} sec. respectively. This value of activation energy suggests an involvement of oxygen vacancies for which the activation energy is in the range of 0.7–1.1 eV [Scott and Dawber (2000), Mao et al. (2013),Ti et al. (2015), Singh et al. (2010)B]. Dielectric behaviour of SFN ceramic was investigated by earlier group also [Raevski et al. (2003), Saha and Sinha (2006)] and they reported that it exhibits high dielectric permittivity resulting from the involvement of the Maxwell-Wagner mechanism [Wang et al. (2017)]. However, recently, Liu et al. (2007) have studied the temperature dependent dielectric characteristics of SFN ceramic samples annealed in O_2

atmosphere. They have reported that the dielectric relaxation occurring in the lower temperature region below room temperature is insensitive to O_2 atmosphere annealing, while the one, occurring in high temperature region above room temperature is sensitive to O_2 annealing. They attributed the low temperature dielectric relaxation to thermally activated intrinsic process induced by local charge ordering while the one in the high temperature region to the thermally activated extrinsic process caused by defect ordering [Liu et al. (2007)].

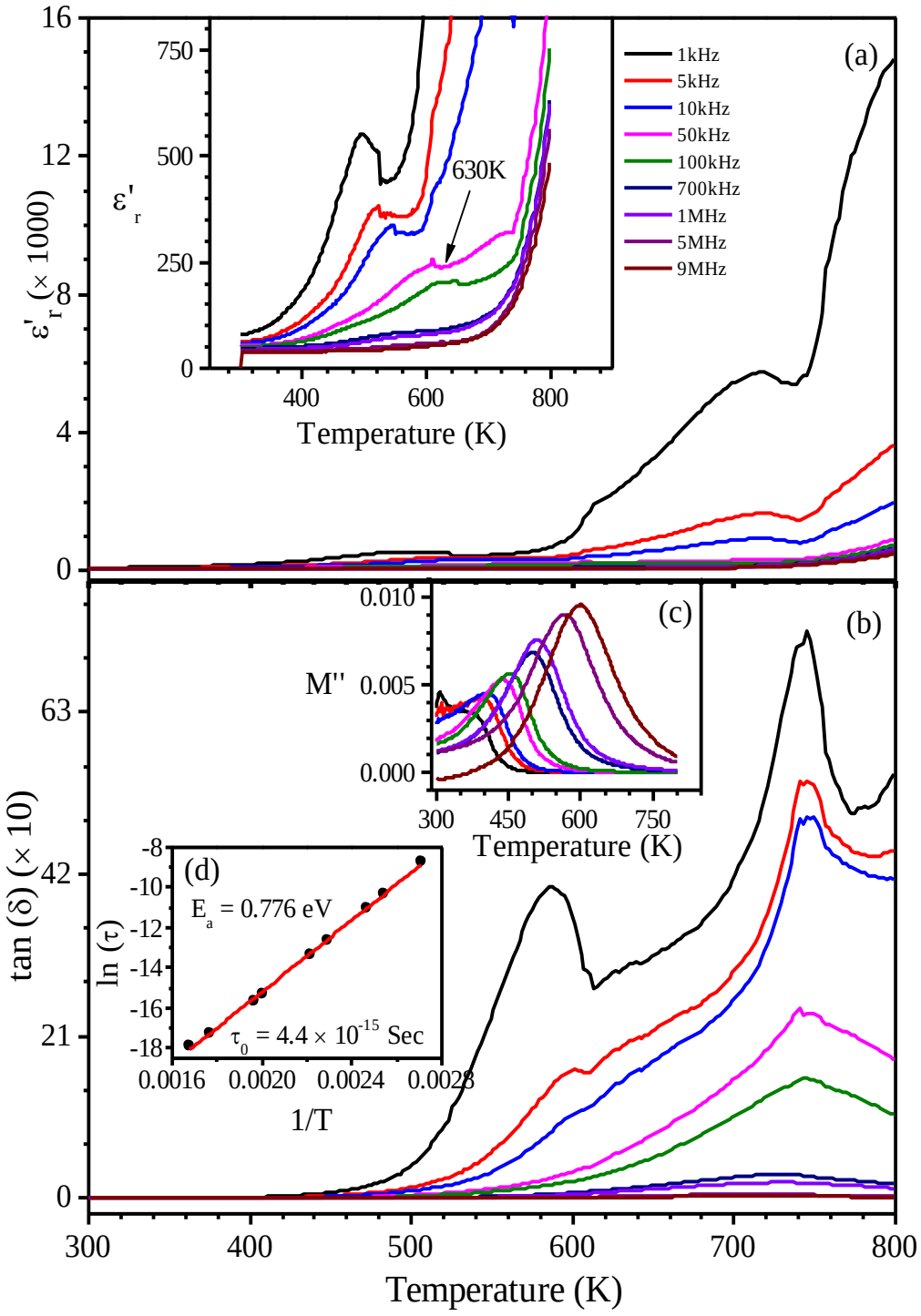

Figure 3.4 Temperature dependent variation of (a) real part of permittivity (ε_r'), (b) loss tangent tan (δ) and (c) modulus (M″) for $Sr(Fe_{0.5}Nb_{0.5})O_3$ ceramic. Arrhenius fit for the dielectric relaxation is shown in (d). The insets to figure (a) shows zoomed portion of real part of permittivity (ε_r').

In our investigation also, the temperature dependent dielectric measurement, in the temperature range 300K to 800K, shows two dielectric relaxations. The first relaxation towards the lower temperature side occurs with large frequency dispersion and is similar to that reported by [Liu et al. (2007)] while the second one in the higher temperature region has less frequency shift and has not been investigated by earlier authors.

3.3.3 High Temperature Magnetic Phase Transition in $Sr(Fe_{0.5}Nb_{0.5})O_3$ Ceramic

Fig. 3.5 (a) and (b) show the temperature dependent plot of the dielectric loss tan(δ) for two frequencies and magnetisation M(T), respectively. Inset to Fig. 3.5(a) shows the magnetic field (H) dependent magnetisation (M) measurement at room temperature. The magnetic hysteresis loop is open up to the field of approximately 6000 Oe. From clearly open M-H loop, it is evident that the magnetic moments of Fe^{3+} ions are not completely antiparallel to each other in super exchange interactions discussed in chapter 1 for magnetic behaviour of such oxides. As shown in Fig. 3.5(a), temperature dependence of tan(δ) measured at 5MHz and 9MHz clearly shows a peak around ~708K. Further, the temperature dependence of magnetization M(T) shown in Fig. 3.5(b) exhibit a magnetic transition around ~708 K. The temperature dependence of first derivative of dc magnetization (dM/dT) shows a clear dip around the magnetic transition temperature ~ 708K as shown in the inset to Fig. 3.5(b). Coincidence of magnetic transition temperature and dielectric loss anomaly temperature suggests that there must be some correlation between magnetic response and the dielectric loss of the material. As shown earlier, the activation energy (0.776 eV) for the dielectric relaxation process is comparable to the activation energy for the oxygen vacancies, which suggests that the dielectric relaxation is mediated through oxygen vacancies [Scott and Dawber (2000), Mao et al. (2013),Ti et al. (2015), Singh et al. (2010B)].

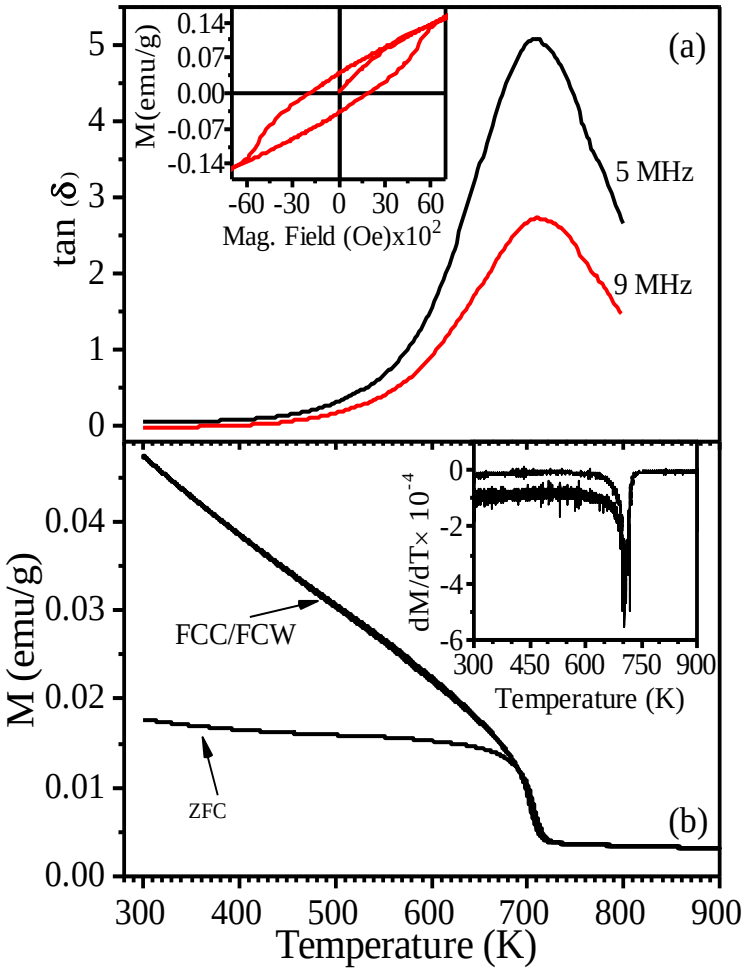

Figure 3.5 Temperature dependence of **(a)** tanδ at frequencies 5MHz and 9MHz **(b)** zero field cooled (ZFC), field cooled cooling (FCC), field cooled warming (FCW) magnetization M(T) of $Sr(Fe_{0.5}Nb_{0.5})O_3$ ceramic sample. Inset to figure (a) and (b) show the magnetization (M) versus magnetic field (H) hysteresis loop and first derivative (dM/dT) of magnetization curve, respectively.

As the super-exchange interaction between Fe^{3+} ions will be mediated by oxygen ions in SFN, formation of oxygen vacancies will play very important role in controlling the magnetic properties [Harrell et al. (2017)]. It is reported for perovskite systems with multiple valences for B-site cations that changes in the oxygen content can change the valence states of the B-site cation to neutralise the excess charge, leading to the tuneable physical properties in such systems [Enriquez et al. (2016)]. Thus formation of oxygen vacancies in SFN may reduce some of the Fe^{3+} ions into Fe^{2+} ions which can

lead to double exchange interactions between Fe^{3+} and Fe^{2+} ions leading to weak ferromagnetic character in the system. It is well known that oxygen vacancies in perovskites, specially containing transition metal cations, significantly alter the spin-orbital coupling and crystal band structures, leading to various unusual electric and magnetic properties [Shuai et al. (2011), Lee et al. (2016)]. Recently it has been reported that oxygen vacancies can remarkably boost the migration of oxygen ions [Enriquez et al. (2015), Bao et al. (2014)] and hence enhance the conductivity that can be seen from the temperature dependent loss tangent tan (δ) plot in Fig 3.4(b). Moreover, since the strength of the magnetic coupling is proportional to the overlap between the contributing orbitals, [Hoffmann et al. (2015), Hoffmann et al. (2018)] oxygen vacancies play the major role in determining the magnetic exchange via Fe-O-Fe chain that drives the magnetic transition. Based on the above, it may be concluded that the magnetic transition observed in our M(T) measurement at temperature (T_M~708K), which is coincident with the dielectric loss tangent anomaly is induced by oxygen vacancies.

3.3.4 X-ray Photoelectron Spectroscopic Studies on $Sr(Fe_{0.5}Nb_{0.5})O_3$ Ceramic

As discussed in earlier section, the significant magnetic moment in the SFN possibly comes out from the double exchange interactions between Fe^{2+} and Fe^{3+} ions. To verify that oxygen vacancies and both the oxidation states of Fe-ions are present in the sample, we carried out X-ray Photoelectron Spectroscopic (XPS) studies. The XPS spectra recorded for Fe- 2p core level and O- 1s core level are shown in Fig. 3.6 (a) and (b). The peaks were calibrated in reference to the C-1s peak appearing at the binding energy of ~ 284.6eV. The deconvolution of XPS spectra was performed by considering a mixture of Gaussian and Lorentzian profile functions in the XPSPEAK software of version 4.1 [Kwok (2000)]. To fit the observed XPS data of Fe-2p core level, the

deconvolution spectra requires number of peaks as reported by [Tang et al. (2015)]. The deconvoluted spectrum of Fe-2p core level for SFN is shown in Fig. 3.6(a). The first two peaks at the binding energy of ~710.3eV and ~712.4eV [Singh et al. (2015)] are due to Fe^{2+} and Fe^{3+} ions in the $2P_{3/2}$ state, the next two and the last one are satellite reflections while the remaining two peaks around ~723.5eV and ~725.5eV [Singh et al. (2015)] are due to binding energies for Fe^{3+} and Fe^{2+} ions in the $2P_{1/2}$ state.

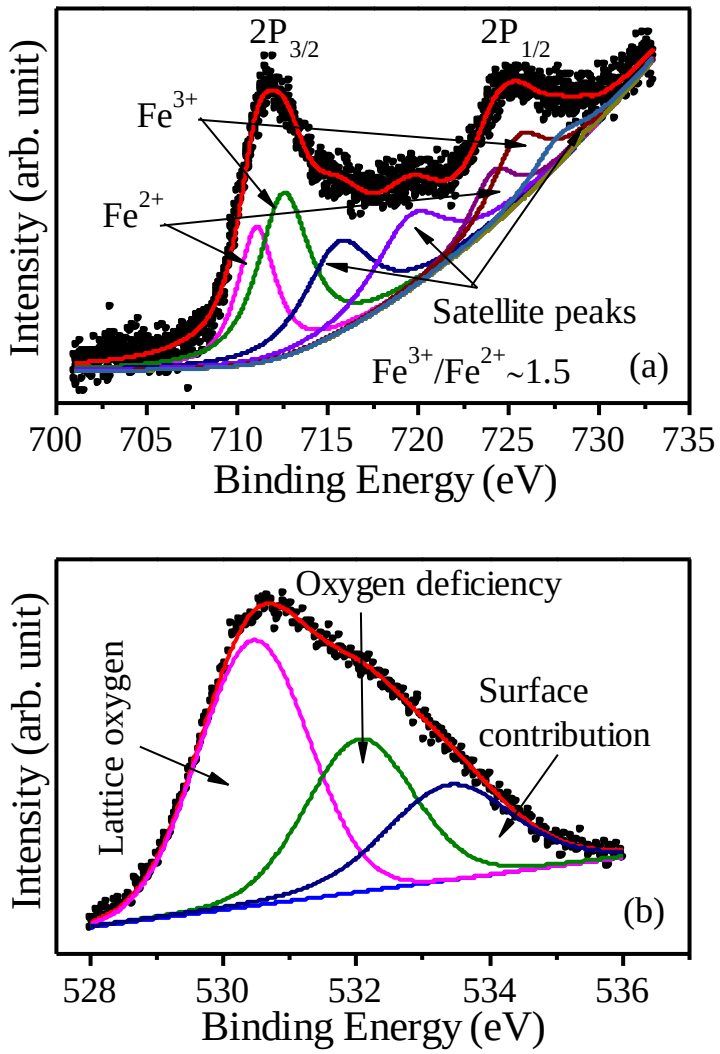

Figure 3.6 The XPS spectra of the Fe-2p level and O-1s level for $Sr(Fe_{0.5}Nb_{0.5})O_3$ ceramic showing presence of oxygen vacancies and Fe^{2+}/Fe^{3+} ions. Experimental data (Black dots), overall fitted curve (red curve overlapping to observed data) and deconvoluted peaks corresponding to various contributions.

The ratio of Fe^{3+} to Fe^{2+} ions calculated from the deconvoluted peaks comes out to be ~ 1.5. This shows that iron ion in the SFN ceramic with the oxidation states of +2 and +3 has approximately 40% and 60% concentrations, respectively. This confirms the results of magnetic measurement discussed in section 3.3.3 that the magnetic contribution to the SFN is coming from the double exchange interaction of Fe^{2+}/Fe^{3+} ions. In addition, the deconvolution of XPS spectra of O-1s core level of SFN ceramic requires three peaks as shown in Fig. 3.6(b). The peak with the lower binding energy ~530.3eV corresponds to the lattice oxygen associated with the Fe^{3+} ion. The middle peak centered at the binding energy of ~ 531.8eV characterise the oxygen deficiency in the SFN lattice. The third peak at 533.3eV is caused by the chemisorbed oxygen lying on the surface of the samples [Mishra et al. (2013), Dohcevic-Mitrovic et al. (2015)].

3.3.5 High Temperature Structural Phase Transition in $Sr(Fe_{0.5}Nb_{0.5})O_3$ Ceramic

In section 3.3.1 we have confirmed that the room temperature structure of SFN ceramic is tetragonal in *I*4*/mcm* space group. For detailed study of the high temperature structural phase transition (also its nature) and it's any correlation with the dielectric/magnetic responses; we carried out high temperature XRD measurements in the temperature range 300 to 850K. The data were recorded at 300, 400, 500, 600, 650, 675, 700, 725, 750, 800 and 850K. Fig. 3.7 shows part of the XRD patterns with 111, 200 and 220 pseudocubic peaks along with superlattice reflection (designated by letter S) at some selected temperatures from 300K to 850K. As discussed in section 3.3.1, the $(200)_{pc}$ and $(220)_{pc}$ profiles are doublet for *I*4*/mcm* space group. The splitting of $(200)_{pc}$ and $(220)_{pc}$ reflections shown in Fig.3.7 decreases with increasing temperature and disappears at and above 650 K.

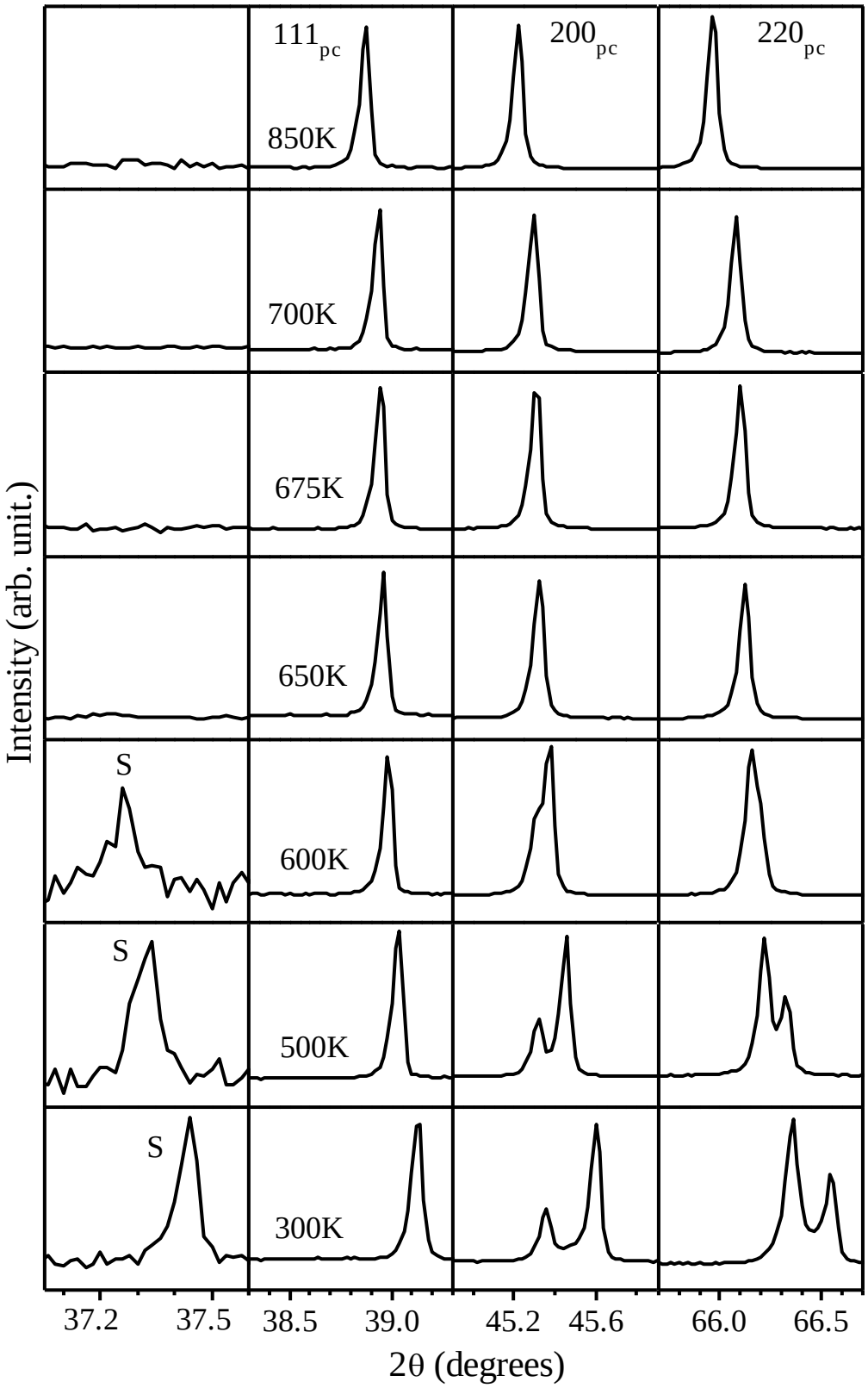

Figure 3.7 Evolution of the pseudocubic 111_{pc}, 200_{pc} and 220_{pc} XRD profiles of $Sr(Fe_{0.5}Nb_{0.5})O_3$ ceramic at various temperatures 300, 500, 600, 650, 675, 700 and 850 K showing structural phase transition near ~ 650 K. The superlattice reflection is marked by letter 'S'.

It is also seen from Fig. 3.7 that the intensity of superlattice peak gradually decreases with temperature and disappear at 675 K. In the diffraction profile recorded at 650 K, the intensity of superlattice peak is barely visible while no splitting is observed in 200 and 220 pseudocubic reflections. This indicates that SFN undergoes a structural phase transition in between the 600 and 650 K temperatures. For detailed structural characterization of high temperature phase transition, we carried out Rietveld structure refinement of the SFN using XRD data from room temperature to 850 K. In Fig. 3.8, we show the observed; Rietveld calculated and difference profiles of some pseudo cubic reflections like 200, 220 and 222 obtained after full pattern Rietveld analysis of XRD pattern recorded at different temperatures. The Rietveld refinement confirms that structure remains tetragonal in space group *I4/mcm* from room temperature to 600 K. Since diffraction pattern collected at or above 650 K, do not show splitting of diffraction peaks or superlattice reflections, we considered cubic structure in $Pm\bar{3}m$ space group for the Rietveld analysis of these diffraction patterns. In the cubic structure with $Pm\bar{3}m$ space group, Sr occupies 1a sites at (0, 0, 0), Fe/Nb on 1b sites at (0.5, 0.5, 0.5) and the oxygen on 3c sites at (0, 0.5, 0.5). As shown in Fig. 3.8, there is very good agreement between the Rietveld calculated and observed XRD patterns. The full pattern Rietveld fits for the diffraction patterns at four representative temperatures are shown in Fig. 3.9. The overall fit of these XRD patterns is also very good.

After successful structural analysis of the X-ray diffraction patterns at various temperatures, we examined the temperature variation of pseudocubic lattice parameters and primitive unit cell volume as shown in Fig. 3.10. It is evident from Fig. 3.10(a) that, as the temperature increases, the ‘a’ and ‘c’ lattice parameters of the tetragonal phase also increase continuously but come closer to each other and finally merge together at transition temperature of 650 K.

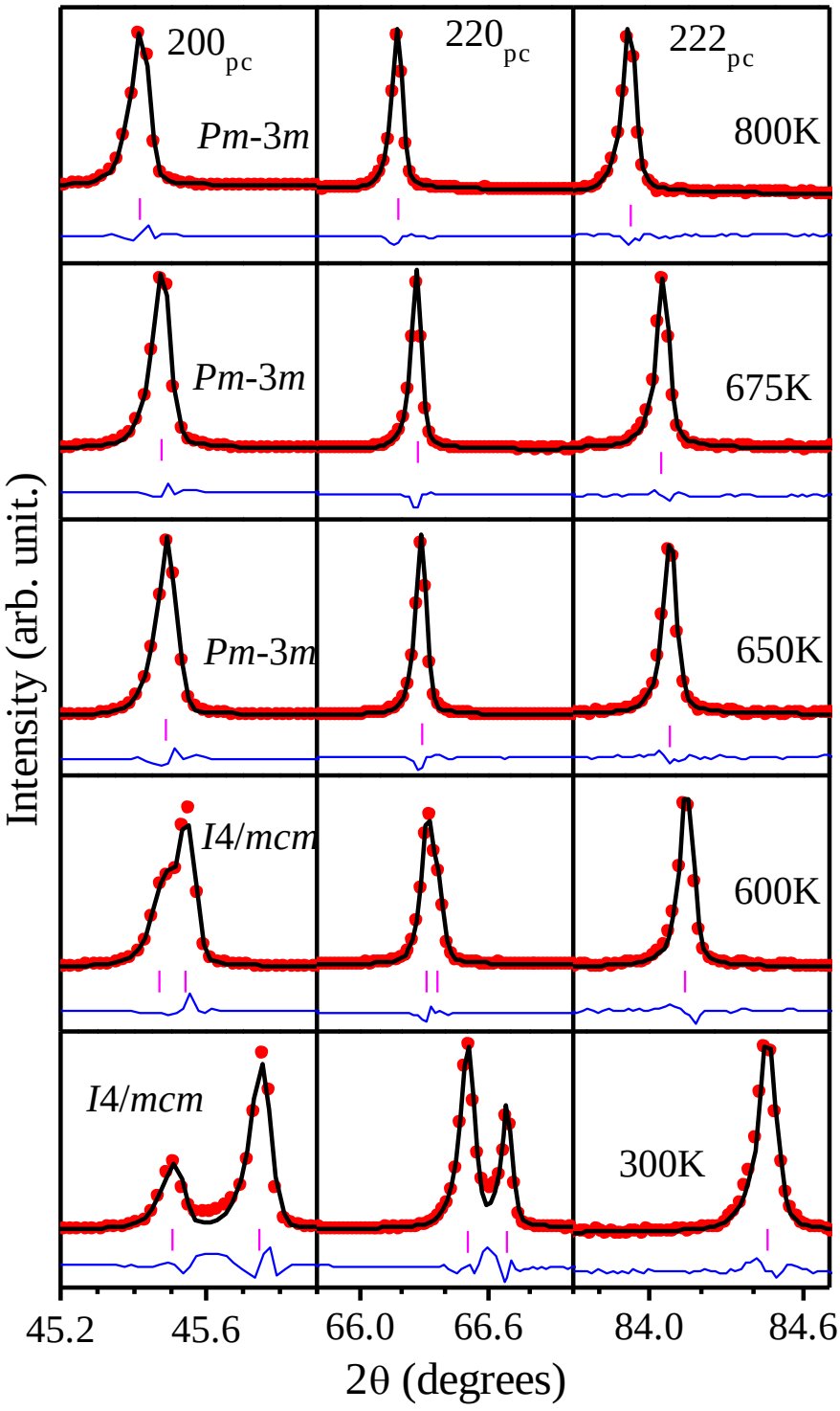

Figure 3.8 Observed (dots), Rietveld calculated (overlapping continuous plot) and difference (bottom curve) XRD profiles for some selected pseudocubic reflections 200, 220 and 222 obtained after full pattern structure refinements using various structural models, *I4/mcm* at 300 to 600 K and $Pm\bar{3}m$ at 650 K to 800 K for $Sr(Fe_{0.5}Nb_{0.5})O_3$ ceramic. Vertical bars are the Bragg's peak positions.

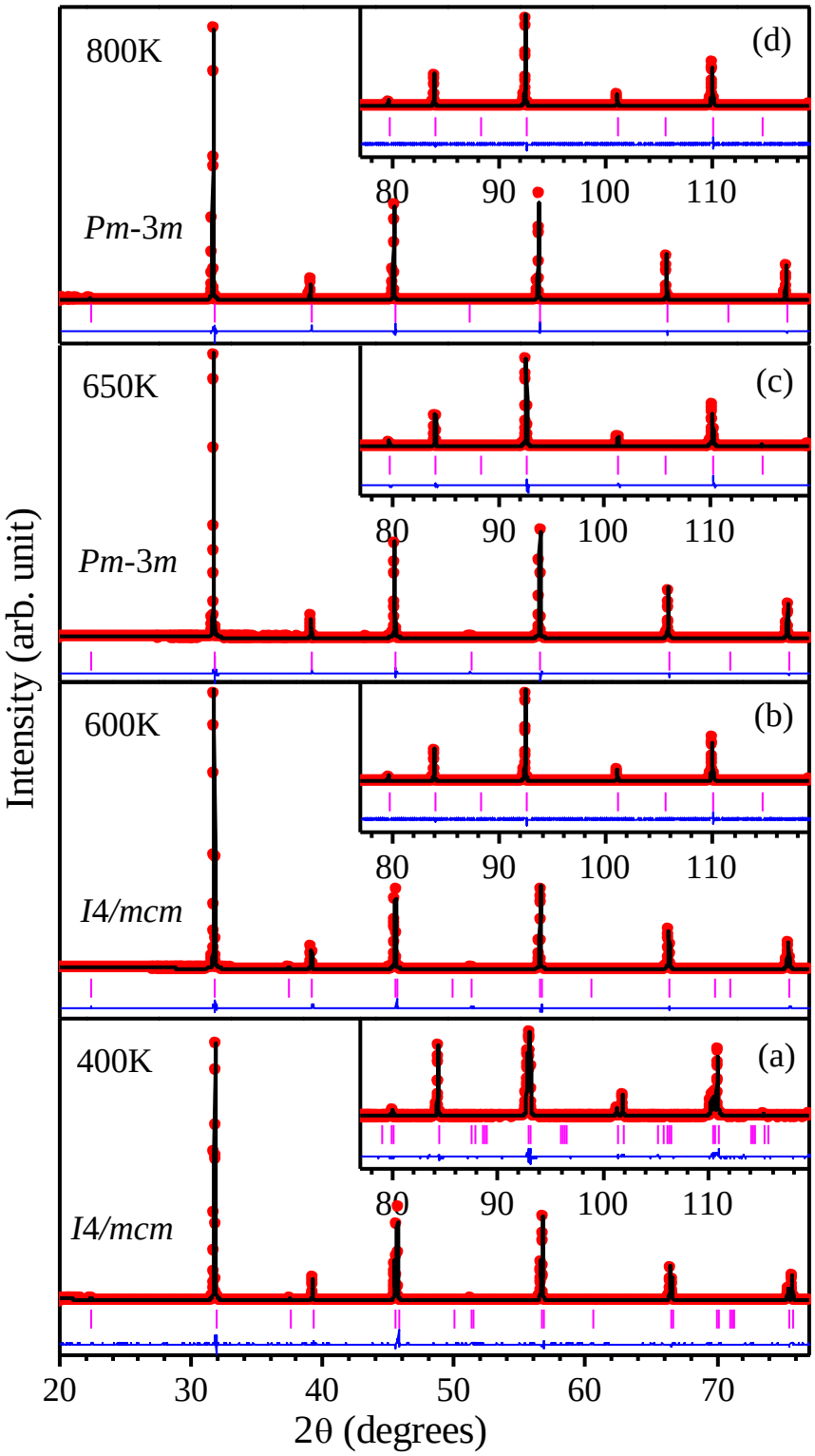

Figure 3.9 Observed (dots), Rietveld calculated (overlapping continuous plot) and difference (bottom curve) XRD profiles obtained after full pattern Rietveld structure refinement of $Sr(Fe_{0.5}Nb_{0.5})O_3$ ceramic using tetragonal *I4/mcm* space group at temperatures (a) 400 K, (b) 600 K and cubic $Pm\bar{3}m$ space group at temperatures (c) 650 K, (d) 800 K. Vertical bars are the Bragg's peak positions.

The transition from tetragonal phase in *I4/mcm* space group having tilt system ($a^oa^oc^-$) to cubic phase in space group $Pm\bar{3}m$ without any tilt ($a^oa^oa^o$) is allowed to be continuous by Landau theory [Howard and Stokes (1998)]. We observe a smooth and continuous variation in primitive unit cell volume across the transition temperature as shown in Fig. 3.10(b). On the basis of above results we can conclude that the tetragonal (*I4/mcm*) to cubic ($Pm\bar{3}m$) phase transformation is of second or higher order.

For the investigation of the nature of structural phase transition, we have studied the variation of oxygen octahedra tilt angle (φ) and the value of integrated intensity (I_{SL}) of the strongest superlattice reflection in the tetragonal phase as a function of temperature. We calculated the tilt angle for oxygen octahedra using the formula ($\varphi = \tan^{-1}4\delta$), where 'δ' is the shift of oxygen atom from their equivalent cubic positions. In Fig. 3.10(c) and 3.10(d), we show the temperature dependence of tilt angle (φ) and the integrated intensity of superlattice peak (I_{SL}). The data points are shown by dots and continuous line is the fitted curve. Both the tilt angle (φ) and the value of I_{SL} decrease continuously and tend to zero as temperature approaches to the structural phase transition temperature. We have found that the tilt angle (φ) and the value of integrated intensity are well described by the expressions $\varphi = B(T_c-T)^{\beta}$ and $I_{SL} = B(T_c-T)^{2\beta}$ [Whitfield et al. (2016)] respectively, where 'B' is a constant, T_c is tetragonal to cubic transition temperature and β is critical exponent. After fitting the data points for tilt angle, we found the value of transition temperature $T_c = 628 \pm 7$K, the value of critical exponent $\beta = 0.247$ and the value of the constant B = 1.42. Moreover, from the fitting of temperature variation of intensity of superlattice peak, we get $T_c = 623 \pm 2$K and $\beta = 0.24$.

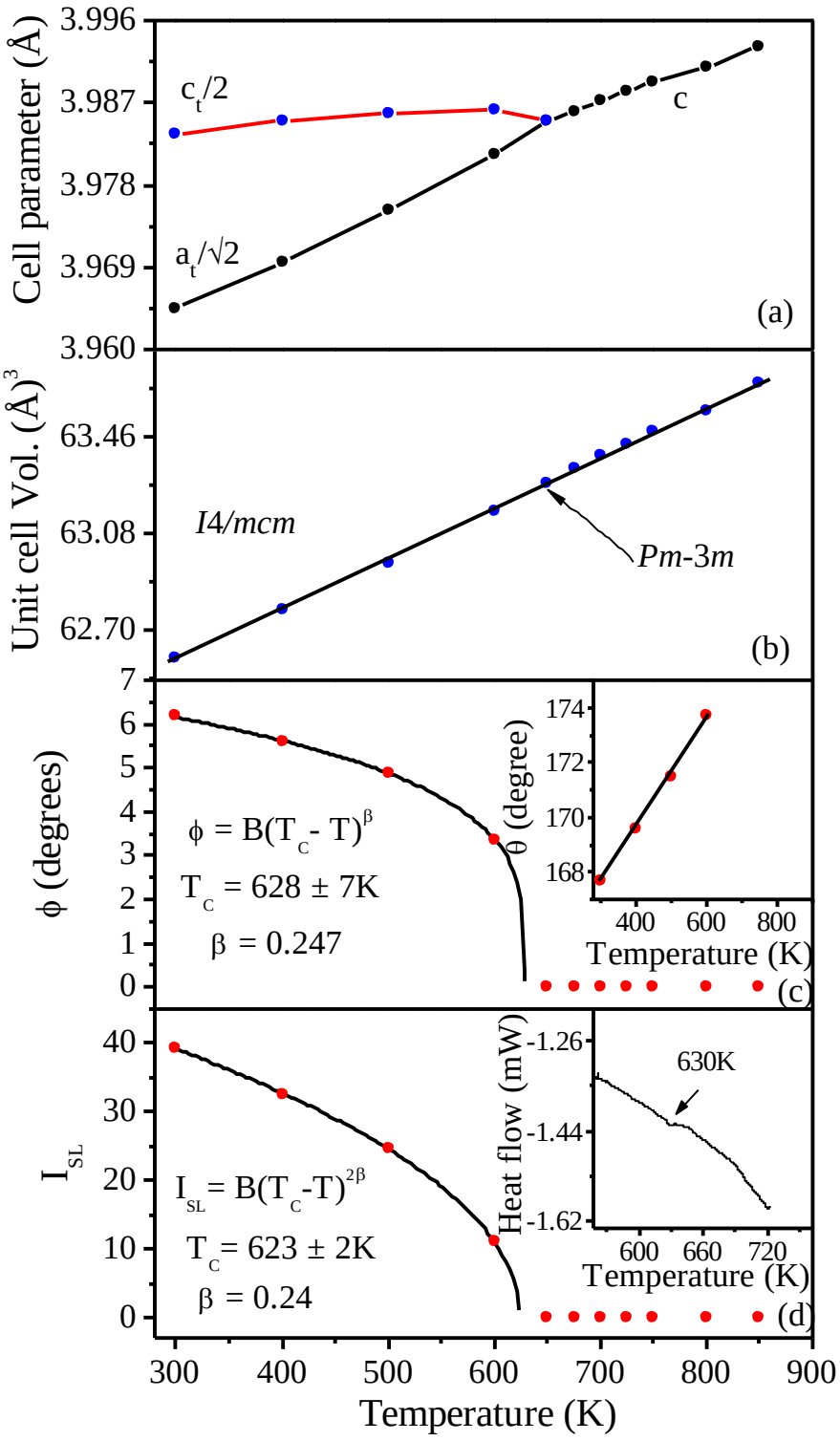

Figure 3.10 Temperature dependent variation of (a) lattice parameters (b) primitive unit cell volume and (c) Fe/Nb-O_6 octahedral tilt angle (φ) (d) Integrated intensity (I_{SL}) of superlattice reflection at 37.5° for $Sr(Fe_{0.5}Nb_{0.5})O_3$ ceramic. Insets to (c) and (d) show temperature variation of Fe/Nb-O-Fe/Nb bond angle (in degrees) and heat flow results respectively. A clear dip corresponding to phase transition is marked by arrow in the heat flow curve.

The structural phase transition temperature (573K) from tetragonal to cubic phase for SFN reported by Lufaso et al. (2006) is 57K lower than our results. This is attributed to the presence of impurity and non-stoichiometric nature of the samples investigated by these authors. In the description of Landau theory, this transition can be second-order as the tetragonal space group (*I*4*/mcm*) is a subgroup of cubic space (*Pm*$\bar{3}$*m*) group [Wilson and Hahn (1983-1995)]. The value of exponent 'β' is very close to 0.25, a characteristic of the presence of a tricritical point, where the fourth order term vanishes in landau potential energy function [Salje (1990)]. $SrZrO_3$ [Kennedy et al. (1999)(A)] and certain other materials having perovskite structure showing this type of behaviour have been reported in literatures [Whitfield et al. (2016),, Carpenter and Salje (1998),, Kennedy et al. (1999)(B)]. The tricritical behaviour for *I*4*/mcm* to *Pm*$\bar{3}$*m* transition can be explained by including sixth order term in the expression for the Landau potential energy function [Salje (1990)]. Since Landau theory denies for the phase coexistence region near tricritical point [Tolenado and Tolenado (1987)], absence of any phase coexistence in our structural studies is well in order. Such variation of tilt angle (φ) is a common feature of tricritical phase transitions [Salje (1990)] and this indicates towards the negligibly small coefficient of the fourth power of order parameter in the expression of Landau potential energy function. Inset to Fig. 3.10(c) shows the temperature dependence of Fe/Nb-O(2)-Fe/Nb bond angle which tends towards 180^0 as the temperature approaches towards transition temperature. Temperature dependence of Fe/Nb-O bond lengths shown in Fig. 3.11 also shows a discontinuous change at the phase transition temperature. The temperature dependent measurement of heat flow of the $Sr(Fe_{0.5}Nb_{0.5})O_3$ ceramic shown in inset to Fig. 3.10(d) also shows a clear dip around 630K, corresponding to the tetragonal to cubic phase transition temperature (T_c).

This provides strong confirmation of the structural phase transition consistent with the X-ray diffraction studies

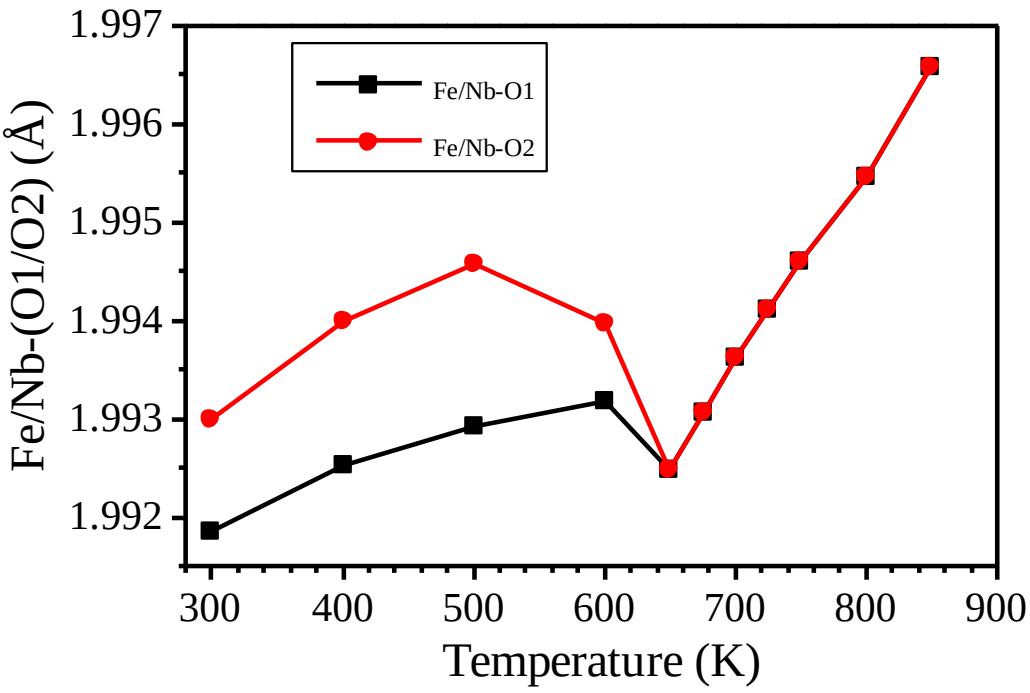

Figure 3.11 Temperature dependent variations of Fe/Nb-O1 and Fe/Nb-O2 bond lengths for $Sr(Fe_{0.5}Nb_{0.5})O_3$ ceramic. The Fe/Nb-O bond lengths become equal in cubic phase.

3.4 Conclusions

We have resolved the controversies about the crystal structure of $Sr(Fe_{0.5}Nb_{0.5})O_3$ ceramic at room temperature. Using Rietveld structure refinement, the correct crystal structure is settled as tetragonal with *I4/mcm* space group. The tetragonal structure (*I4/mcm*) transforms to cubic structure ($Pm\bar{3}m$) around ~630K as confirmed by the temperature dependence of heat flow measurement (DSC), FeO_6 octahedra tilt angle (ϕ) and integrated intensity (I_{SL}) of strongest superlattice reflection. The value of critical exponent ($\beta \sim 0.25$) for the temperature variation of octahedral tilt angle (φ) and the integrated intensity of superlattice reflection (I_{SL}) for SFN ceramic confirm tricritical

nature of structural phase transition. A new magnetic phase transition is discovered around ~708K which is well above the structural phase transition temperature ~630K. The XPS studies of the Fe-2p core level and O-1s core level of $Sr(Fe_{0.5}Nb_{0.5})O_3$ ceramic confirm the presence of oxygen vacancies as well as Fe ions in the +2 and +3 oxidation sates. The significant magnetization in $Sr(Fe_{0.5}Nb_{0.5})O_3$ ceramic results from ferromagnetic contributions coming from the double exchange interactions in Fe^{2+}-O-Fe^{3+} chains.